POLITECNICO DI TORINO
Repository ISTITUZIONALE

Alkali-activation of aggregate fines from construction and demolition waste: valorisation in view of road pavement subbase applications

Original
Alkali-activation of aggregate fines from construction and demolition waste: valorisation in view of road pavement subbase applications / Bassani, M.; Tefa, L.; Coppola, B.; Palmero, P.. - In: JOURNAL OF CLEANER PRODUCTION. - ISSN 1879-1786. - STAMPA. - 234:(2019), pp. 71-84. [10.1016/j.jclepro.2019.06.207]

Availability:
This version is available at: 11583/2738212 since: 2019-07-21T19:59:56Z

Publisher:
Elsevier

Published
DOI:10.1016/j.jclepro.2019.06.207

Terms of use:

This article is made available under terms and conditions as specified in the corresponding bibliographic description in the repository

Publisher copyright
Elsevier postprint/Author's Accepted Manuscript

© 2019. This manuscript version is made available under the CC-BY-NC-ND 4.0 license
http://creativecommons.org/licenses/by-nc-nd/4.0/.The final authenticated version is available online at:
http://dx.doi.org/10.1016/j.jclepro.2019.06.207

(Article begins on next page)

18 April 2024

ALKALI-ACTIVATION OF AGGREGATE FINES FROM CONSTRUCTION AND DEMOLITION WASTE: VALORISATION IN VIEW OF ROAD PAVEMENT SUBBASE APPLICATIONS

Bassani[1]*, M., Tefa[1], L., Coppola[2], B., Palmero[2], P.

([1]) Department of Environment, Land and Infrastructures Engineering

([2]) Department of Applied Science and Technology

Politecnico di Torino, Torino, Italy

Marco Bassani (* = *corresponding author*): +39 011 090 5635, E-mail: marco.bassani@polito.it

Luca Tefa: +39 011 090 5623, E-mail: luca.tefa@polito.it

Bartolomeo Coppola: +39 011 090 4678, E-mail: bartolomeo.coppola@polito.it

Paola Palmero: +39 011 090 4678, E-mail: paola.palmero@polito.it

ABSTRACT

This study investigates the potential of fine particles of recycled construction and demolition waste (CDW) aggregate to undergo alkali-activation when mixed with an appropriate alkaline solution. The fine is a natural by-product of the milling process and includes particles from four main material sources (i.e., recycled concrete, recycled asphalt, crushed bricks and tiles, and natural aggregate and excavated soil) and other occasional elements which are too small for identification. The fine was obtained by sifting the material through a 125 μm sieve. Since the reactivity of unselected material depends on its constituents, these were also individually investigated. Firstly, the four constituents of CDW recycled aggregates were separated, then milled to a size smaller than 125 μm, before being tested to measure their reactivity to an alkaline solution. A preliminary chemical and mineralogical characterization of the five powders was carried out to identify the main crystalline phases and ascertain the presence of aluminosilicates needed for the alkali activation process. Particles of each powder were afterwards mixed with three concentrations of the same alkaline solution with a liquid/solid mass ratio of 0.4, cast in prismatic moulds, and cured at room temperature. Mechanical tests after 3, 7, and 28 days of curing demonstrated that powders react positively in a basic environment, showing an increase in strength without any thermal treatment. Hardened pastes of undivided fine aggregate and recycled asphalt exhibited the best results in terms of flexural and compressive strength with the more concentrated solution. A Field Emission Scanning Electron Microscopy analysis was also carried out to observe the microstructure and to support an interpretation of the mechanical strength data. Results demonstrated the feasibility of using a solution to activate unselected CDW fine particles to stabilize CDW aggregates. In full scale applications, CDW aggregates can be stabilized without the addition of any binder.

KEYWORDS: construction and demolition waste, alkali-activation, constituents, stabilization, composition properties relationship, compressive and flexural strength.

HIGHLIGHTS

1. An investigation into alkali-activated recycled aggregate fines from construction and demolition waste (CDW)
2. Reactivity of powders produced by the sieving of CDW and the milling of CDW constituents was assessed
3. Particles mixed with three different concentrations of an alkaline solution with a liquid/solid ratio of 0.4
4. Mechanical tests at 3, 7, and 28 days of curing show an increase in strength at room temperature
5. In subbase applications CDW aggregates can be stabilized without the addition of industrial binders

1. INTRODUCTION

The continuous production of waste from construction and demolition activities is a major environmental concern in European countries. EU Commission estimates reveal that construction and demolition waste (CDW) accounts for approximately 25-30% of all waste generated in Europe (European Commission, 2011). Several researches have demonstrated the potential for the reuse of this waste as an alternative material in civil engineering (Cardoso et al., 2016; Contreras et al., 2016; Vieira and Pereira, 2015). This is due to the presence of solid particles from a variety of construction materials which can form new aggregate grains of variable toughness and hardness, depending on composition, which in turn is conditioned by the type of construction and/or demolition work. In fact, an unselected CDW usually includes constituent materials in different proportions including (recycled) concrete fragments (RC), ceramic products such as crushed bricks and tiles (BT), reclaimed asphalt pavement grains (RA), natural aggregates and excavated soils (NA), together with occasional small particles of glass, wood, metals, and plastic (Jiménez, 2013).

Member states are being encouraged by the European Directive 2008/98/EC (European Parliament, 2008) to increase the use of recycled non-hazardous waste resources in place of natural materials to a minimum of 70% (by weight) by 2020. Consequently, construction activity has witnessed the increased use of alternative materials and recycled aggregate from CDW in numerous civil works (Vandecasteele et al., 2013).

Different studies compared the physical and mechanical properties of CDW aggregates to those containing natural aggregates, concluding that they can be employed in non-structural concrete applications (Silva et al., 2014; Rodríguez et al., 2016; Juan-Valdés et al., 2018) and also, albeit in limited percentages, in structural (Tsoumani et al., 2015; Pitarch et al., 2017) and high-performance concrete (Limbachiya et al., 2000; Gonzalez-Corominas et al., 2017). Several investigations demonstrated that unselected CDW can be successfully used as granular material for unbound layers of pavement structures (Ossa et al., 2016; Bennert et al., 2000; Poon and Chan, 2006; Leite et al., 2011; Arulrajah et al., 2013), for layers of low traffic unpaved roads (Jiménez et al., 2012; Del Rey et al., 2016a), in road embankments (Sangiorgi et al., 2015) and trench backfilling (Chen et al., 2017; Rahman et al., 2014) and as aggregate for bituminous mixtures (Gómez-Meijide et al., 2016; Paranavithana and Mohajerani, 2006; Pasandín and Pérez, 2013). This substantial body of literature supports the extensive reuse of CDW aggregates for a cleaner and more sustainable development of new transportation infrastructures, as well as the maintenance of existing ones.

Focalizing on their application to base and subbase layers of road pavements, many authors advocated the possibility of stabilizing CDW aggregates with ordinary Portland cement (Agrela et al., 2012; Mohammadinia et al., 2014; I. Del Rey et al., 2016b) or with alternative binders containing by-products such as fly-ash (Arulrajah et al., 2017), and cement kiln dust (Bassani et al., 2016), with the aim of enhancing their mechanical properties and durability. These ordinary and alternative binders display a different reactive attitude thanks to the presence of water; thus, they can develop the required strength and stiffness in both the short and long term.

Among the alternative binders, alkali-activated binders, usually known as “geopolymers”, certainly merit a mention. Although this technique has been in existence for more than 70 years (Roy, 1999), it has only become common in recent years thanks to the fact that it is more effective than Portland cement in the reduction of greenhouse emissions (Duxson et al., 2007a; McLellan et al., 2011; Jamieson et al., 2015; Nguyen et al., 2018). Alkali-activated binders derive from the chemical reaction between precursors (normally aluminosilicate powders) and alkaline activators (normally mixtures of sodium hydroxide and sodium silicate). Alkaline activation (AA) entails the dissolution of solid aluminosilicates in an alkali medium, the transportation of dissolved species, and the polymerization of silica and alumina tetrahedra in a continuous three-dimensional network (Komnitsas and Zaharaki, 2007; Duxson et al., 2007b).

Several recent contributions refer to the chemical stabilization of CDW aggregates by the AA process with the addition of amorphous, highly reactive components such as fly ash (FA) (Hoy et al., 2016), ground granulated blast furnace slag (GGBFS) (Mohammadinia et al., 2016; Arulrajah et al., 2016), and calcium carbide residue (Arulrajah et al., 2016). These contributions have all demonstrated that the addition of reactive components results in a significant enhancement of the mechanical properties of recycled materials in terms of strength (i.e., unconfined compressive) and stiffness (i.e., resilient modulus) independently of the curing temperature (between 20 and 40°C). Hoy et al. (2016) also observed that the strength of RA and FA geopolymer mixtures increased as the $NaOH/Na_2SiO_3$ ratio decreased. Similar results were obtained with alkali-activated pastes and concretes (Bondar et al., 2019; Humad et al., 2019), and other hazardous, contaminated sediments and soils (Wang et al., 2019a; Wang et al., 2019b).

In current literature, several studies have investigated the AA of powders from CDW, albeit the procedure is confined to cementitious and ceramic components and has always been performed with a thermal treatment to improve final performance (Zaharaki et al., 2016). Komnitsas et al. (2015) demonstrated the potential use of pulverized CDW (including RC and BT) as raw material for the synthesis of alkali-activated cements. High mechanical strength values (more than 50 MPa of compressive strength) were achieved after 7 days of heat curing (90°C) for BT samples, whereas RC powders showed a lower reactivity and lower mechanical performance. Similar results were achieved by (Allahverdi and Kani, 2009), who compared the AA of BT and RC constituents, concluding that BT exhibited better AA behaviour due to the higher aluminosilicate content. Pathak and Jha (2013) used a calorimetric analysis to demonstrate the higher reactivity (i.e., the greater dissolution of aluminosilicate species under alkaline conditions) of BT compared to RC. Robayo-Salazar et al. (2017) demonstrated that the addition of Portland cement (from 0 to 30% in mass) in AA red clay brick mixtures promotes the optimum strength development of specimens cured at room temperature. The experimental investigation carried out by Reig et al. (2013) revealed that ceramic waste materials, when used as precursors for AA mortars, can develop compressive strength values in a range between 21 and 44 MPa, after 7 days of curing at 65°C. Zedan et al. (2015) investigated the effect of mixing ceramic, red clay brick and concrete wastes with GGBFS on the properties of the alkali-activated paste produced. The replacement of 10% (in weight) of the slag with concrete waste increased the compressive

strength for short curing times. In contrast, for longer curing times, the mixtures containing ceramic components showed the highest values, suggesting their continuous dissolution in the alkaline medium, providing the system with aluminate and silicate species which completed the geo-polymerization reactions.

This body of research lends support to the possibility of stabilizing selected and unselected CDW aggregates to reach minimum strength and stiffness requirements for stabilized granular materials in base/subbase pavement layer applications (Figure 1a). However, none of the studies commented on here has investigated the possible activation of silica and alumina normally present in the finest particles of unselected CDW aggregates. To pursue this aim, in this study the reactivity of fines from unselected CDW recycled aggregates (named "UND") was studied and results were compared with those of separated constituents (namely, NA, BT, RC and RA) of CDW.

Figure 1 provides the general concept of this investigation, which follows up on a previous work by the authors (Bassani et al., 2019) in which the full mixture consisting of small, coarse particles of an unselected CDW was alkali-activated for stabilization purposes. In that case, the material was first divided into size classes, and then recombined to follow the reference grading curve reported in Figure 1b (CIRS, 2001). In Bassani et al. (2019) the fraction passing at the 0.125 mm sieve was equal to 11.9% (Figure 1b). These fine particles were considered to have the greatest potential for activation by the alkali liquid medium (Komnitsas et al., 2015; Temuujin et al., 2009; Assi et al., 2018) thanks to the presence of significant amounts of silica and alumina. The UND fines were deemed to be responsible for the creation of weak bonds able to stabilize the full unselected CDW mixture made up of coarser particles (the fraction retained at 125 μm sieve) and fines.

In contrast with previous investigations (Bassani et al. 2019), the aim of this investigation is to assess the alkali-activation rate of UND fines and determine which UND elements are chiefly responsible for triggering their reactivity. The alkali activation of CDW recycled aggregate fines in order to stabilize the whole material without the addition of industrial binders or reactive by-products (i.e., FA, cement kiln dust, GGBFS) does not feature in scientific literature and practical applications, and it is therefore the focus of and, indeed, the innovative feature of this research.

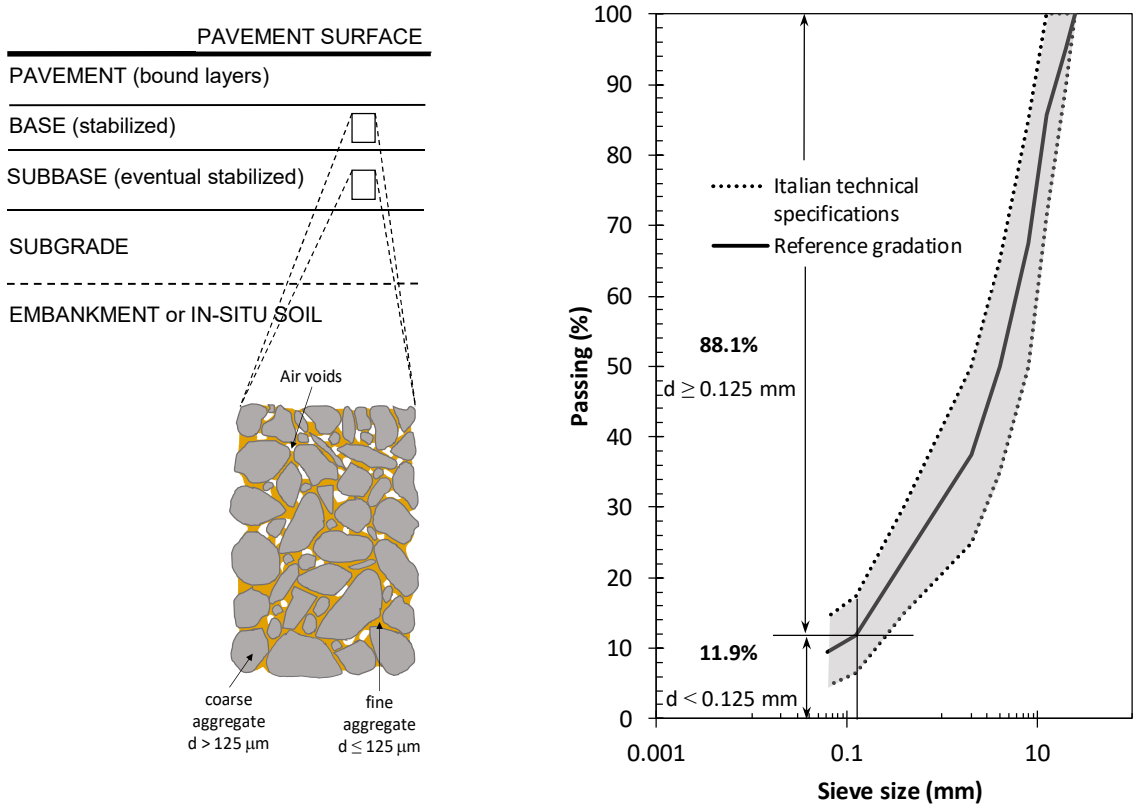

Figure 1. Use of alkali-activated unselected CDW aggregates (Bassani et al., 2019) in the formation of stabilized layers (base and/or subbase) in a typical road pavement system. (a) Function of fine ($d \leq 0.125$ mm) and coarse ($d > 0.125$ mm) particles in the AA stabilized CDW aggregates; (b) mass percentage of fine and coarse aggregates of base/subbase stabilized materials according to Italian specifications (CIRS, 2001) the reference grading curve is the average of the two grading limits.

2. MATERIALS AND METHODS

2.1 Solid particles

A large sample of CDW aggregates, in the 0-25 mm size fraction, was sourced from a plant operating in the Turin area (North West of Italy). UND was obtained by sieving the CDW sample. A smaller 20 kg sample, containing particle sizes of 5-25 mm, was used to obtain the four main constituents (RC, RA, BT, and NA) through the visual identification of each particle. Each fraction was then ground in a rotary drum to obtain fine powders in two different size classes (<63 µm and 63-125 µm). Previous literature underlined that geo-polymerization is affected by particle size distribution: the smaller the size, the quicker the alkali-activation reactions, and thus the higher the final mechanical properties (Assi et al., 2018). It should be noted that the UND consisted of an unknown combination of RC, RA, BT, and NA fines together with minor quantities of unidentified material.

Small quantities of RC, RA, BT, NA and UND particles (smaller than 63 µm) were subjected to X-Ray Diffraction (XRD, Philips PW 1710), to assess the presence of aluminosilicates and differences in crystalline

phases between constituents. In addition to peaks indexing carried out by means of JCPDS (Joint Committee of Powder Diffraction Standards), a semi-quantitative phase analysis was performed by exploiting the Reference Intensity Ratio (RIR) given by the JCPDS files for each identified phase (Zhou et al., 2018), and using the following equation:

$$X_i = 100 \cdot \frac{I_i}{RIR_i \cdot \sum_{j=1}^{n} \frac{I_j}{RIR_j}} \quad \text{(eq. 1)}$$

where X_i is the weight in percentage terms of the phase i; I_i and I_j are the relative intensities for phases i and j; n is the number of crystalline phases in the sample; RIR_i and RIR_j are the reference intensity ratios for phases i and j respectively (corresponding to the ratio of intensity of a peak of the pure phases i and j to the intensity of a peak of the corundum reference phases).

Furthermore, the full chemical composition of the fines was assessed by X-Ray Fluorescence (XRF, Rigaku ZSX 100E) and reported in Section 3.2.

The particle size distribution of both fractions (<63 μm and 63-125 μm) was determined by laser granulometer (Fristch Analysette 22). The particle density was determined by a pycnometer, according to EN 10977 (European Committee for Standardization, 2008a), while the intergranular porosity of dry compacted samples was determined by means of the Rigden compaction apparatus according to EN 10974 (European Committee for Standardization, 2008b). The same device was employed to measure the bulk density of compacted particles. To calculate the volume of the voids of the compacts, the following equation was used:

$$\nu = \left(1 - \frac{4 \cdot 10^3 \cdot m_2}{\pi \cdot \alpha_2 \cdot \rho_f \cdot h}\right) \cdot 100 \quad \text{(eq. 2)}$$

where ν is the intergranular porosity (or Rigden voids, %), m_2 is the mass of the compacted fines (g), α is the internal diameter of the cylinder mould (mm), ρ_f is the volumetric mass of the fines in Mg/m^3, h is the height of the compacted fines (mm). The morphology of the powders was characterized by Field Emission Scanning Electron Microscopy (FESEM, Hitachi S4000, Japan).

2.2 Liquid phase

A mixture of sodium hydroxide (NaOH) and sodium silicate (Na_2SiO_3) was used to prepare the activating solution (AS). The NaOH was in solid form (flakes), so it was dissolved in distilled water to form an aqueous solution at 50% by weight (concentration of 25 M). The Na_2SiO_3 was in liquid form, characterized by a modulus (i.e., the SiO_2/Na_2O molar ratio) of 3.4 and a concentration of about 36%. It was mixed with NaOH solution in a 4:1 mass ratio to produce the AS.

The AS was used in both undiluted and diluted form, with the latter in concentrations of 75% and 50%. Therefore, three different concentrations were employed, labelled as sol_100% (AS without dilution), sol_75%

(AS diluted with 25% of distilled water, i.e. 75% concentration) and sol_50% (AS diluted to 50%) respectively. Figure 2 shows the composition of the three solutions.

The concentration of NaOH in the full AS was 4, 3.5 and 1.5 M for sol_100%, sol_75%, and sol_50% respectively. The AS concentration was varied to investigate its influence on the reaction efficiency, which in turn was assessed in terms of flexural and compressive strength.

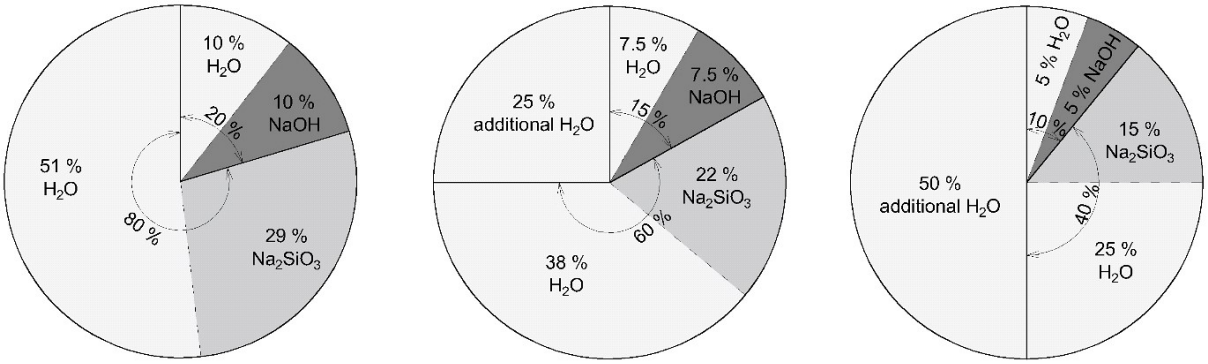

(a) (b) (c)

Figure 2. Composition of the three alkaline solutions: (a) sol_100%, (b) sol_75%, and (c) sol_50%.

2.3 Testing program on solid-liquid mixtures

Each fine (RC, RA, BT, NA and UND) was mechanically mixed with the AS, which played the dual role of chemical activator, and liquid phase to provide the required mixture workability. The two fractions of each constituent were blended with 50% (by weight) of the 63-125 μm fraction, and 50% (by weight) of particles < 63 μm, and then mixed with AS. In all cases, a liquid to solid (l/s) weight ratio of 0.4 was adopted, where the liquid phase corresponds to the AS amount. By considering the three different dilutions of AS, the following water to solid (w/s) weight ratios were achieved: w/s = 0.25 in the case of sol_100%, w/s = 0.28 for sol_75% and w/s = 0.32 for sol_50%.

Mixtures at a second l/s ratio of 0.6 were prepared as well in order to perform rheological measurements using a viscometer (Brookfield HBDVII). After a pre-shear, the apparent viscosity was measured at room temperature at shear rates ranging from 6.12 to 245 s^{-1}, maintaining each value constant for 10 s.

The mixtures were cast into prismatic moulds (80×20×20 mm^3) and cured at room temperature for 3, 7 or 28 days and then subjected to mechanical characterization. The flexural strength was measured on a three-point bending configuration, while the compressive strength was determined on residual pieces of samples derived from the flexural test. A 50 kN electro-pneumatic testing device was used; load and vertical displacement values were recorded at 10 Hz at a deformation speed of 0.25 mm/min. The experimental program included five fines (RC, RA, BT, NA, UND), three AS concentrations (100%, 75%, 50%), three

curing times (3, 7, 28 days), and four replicates, so a total of 180 samples were prepared and tested. The hardened samples, obtained by alkaline activation with sol_100% and cured for 28 days, were finally subjected to FESEM characterization.

3. RESULTS AND DISCUSSION

3.1 Physical properties

Figure 3 reports the particle size distribution of the five samples, sieved in the two different ranges. In the 63-125 μm size range, the five constituents show a similar particle distribution, with a d_{50} value (i.e., the mean diameter of the volume distribution) close to 100 μm. Considering the finer fraction (< 63 μm), RC, BT, NA and UND show a similar average particle size (d_{50} in the range 19-22 μm), while RA distribution is shifted to larger values (d_{50} of about 35 μm), suggesting a less effective milling process. A further difference worth noting is the progressive decrease in d_{90} values, when moving from the larger RA (d_{90} of about 70 μm), to the finer UND sample (d_{90} of about 30 μm). BT, NA and RC showed intermediate values, with d_{90} of about 48, 47 and 37 μm, respectively.

Table 1 collects the particle density (ρ_p), the bulk density (ρ_b), and the porosity of dry compacted powder (v) for each constituent. NA and BT particles showed the highest densities, in accordance with the high mineral content of these fractions. RC was characterized by lower density values, probably due to residues of cement paste adhering to the natural aggregates even after crushing (Katz, 2003). Finally, the lowest values were determined for RA. This behaviour was imputed to bitumen, which makes up approx. 6% of RA (Mhlongo et al., 2014) and is characterized by a significantly lower density around 1010 kg/m^3 (Loria et al., 2009) in comparison to the aggregates used in asphalt mixtures in the range 2200 - 2700 kg/m^3 (Acosta Alvarez et al., 2018).

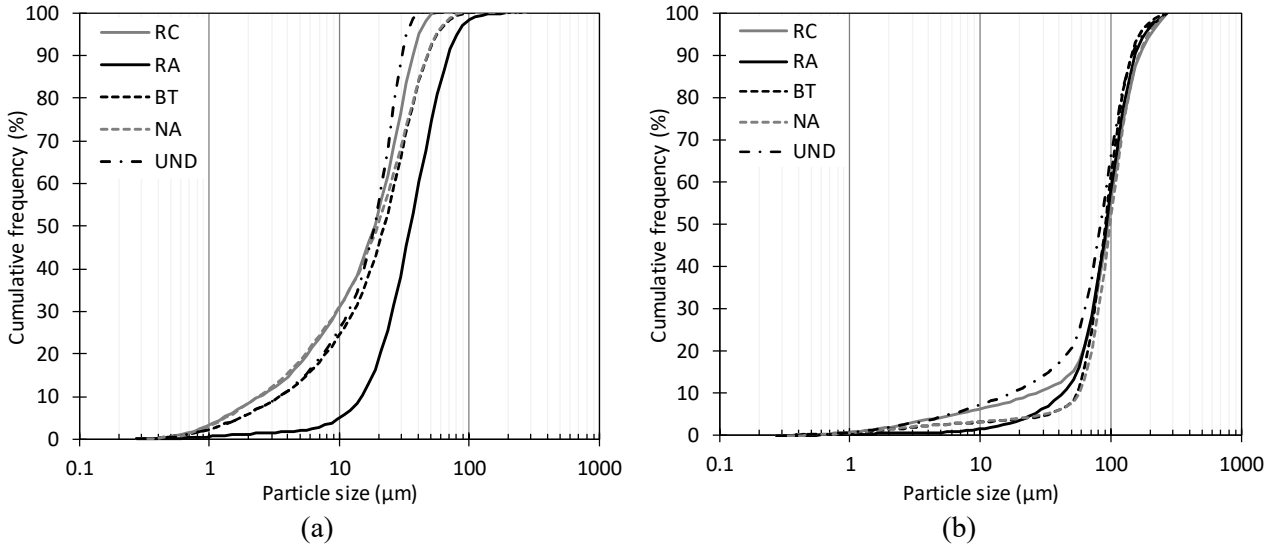

Figure 3. Cumulative particle size distribution of constituents obtained with separate size fractions: (a) < 63 μm, and (b) 63-125 μm.

Table 1. Particle density (ρ_p), bulk density (ρ_b) and Rigden porosity (ν) of constituents for separate size fractions (< 63 μm and 63-125 μm)

Constituent	Particle size [μm]	ρ_p [Mg/m^3]	ρ_b [Mg/m^3]	ν (%)
RC	<63	2.580	1.945	24.6
	63–125	2.687	1.953	27.3
RA	<63	2.424	1.940	20.0
	63–125	2.347	1.990	15.2
BT	<63	2.763	2.010	27.3
	63–125	2.722	1.946	28.5
NA	< 63	2.726	1.987	27.1
	63–125	2.710	2.025	25.3
UND	< 63	2.640	1.963	25.6
	63–125	2.673	1.963	26.5

It is worth noting that the Rigden void values, which indicate the propensity of fines to be compacted at the same compression effort, are normally included in the range 24.6-28.5%, with the exception of RA which is in the range 15.2-20%. On the one hand, this effect can be imputed to the specific size distribution of RA particles (Figure 3) which differ from the other CDW constituents. RC, BT, NA and UND have a higher amount of very fine particles which may result in a higher volume of small spaces between grains. On the other hand, the residual bitumen in RA could act as a plasticizer and binding component (Formela et al., 2016; Kishchynskyi et al., 2016), thus enhancing the compaction behaviour and therefore lowering the porosity amount of the dry sample.

In Figure 4, some representative micrographs of the five components which were sifted through a 63 μm sieve are depicted. In particular, the low magnification images show the particle size distribution of the different fractions. NA presents the finest distribution, while BT and RA present the coarsest. However, it should be specified that the particle sizes in Figures 3a and 4 cannot be directly compared, since the powders used for laser granulometry were dispersed in a liquid medium (distilled water or absolute ethanol), while the FESEM micrographs are taken on dried powders, and thus potentially agglomerated. In Figure 4, higher magnification micrographs are displayed as insets to the main images, in order to illustrate the morphology of some selected particles. In all cases, sharp-edged grains are the result of the crushing and milling processes. However, while NA and BT present a compact structure and the particles have a smooth surface, RC shows an inhomogeneous and porous layer partially covering the single grains. This feature is better evidenced in the higher magnification image of RC, in which this layer has been associated with residual cement paste, partially covering the aggregate surface. A different morphology was observed for RA, since in some cases large agglomerates of primary particles are recognized due to the presence of bitumen, which can act as a binder phase for the finest powders. Finally, the UND micrograph shows a collection of indistinguishable particles, where a quantity of very fine debris can be observed as well, in line with its finer particle size distribution (Figure 3).

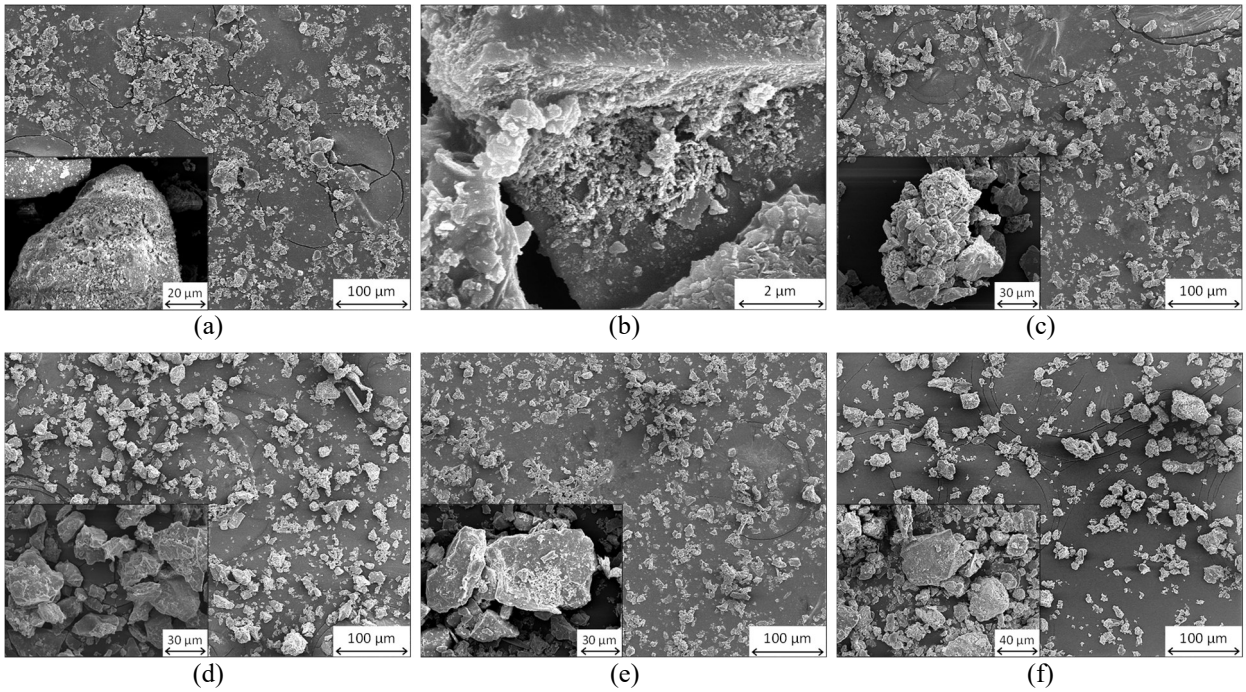

Figure 4. FESEM micrographs of raw materials for alkali activation: (a) RC, (b) RC, (c) RA, (d) BT, (e) NA, (f) UND. Inset to images, a higher magnification micrograph, displaying the morphology of some selected particles. In the case of RC (a), a further higher magnification image (b) is provided to show the cement paste residue on the aggregate.

3.2 Phase composition of constituents

The indexed XRD patterns for the five fines are depicted in Figure 5. XRD results showed that all the fractions were well crystallized. A feature common to all constituents is the presence of quartz, the main peak of which (corresponding to the lattice plane 101 and located at 26.65° 2θ) shows a predominant intensity over the XRD reflections of all other phases. Calcite is also present in all the samples, with a strong peak intensity in RC, a low relative intensity in BT, and an intermediate situation in the other constituents.

Besides quartz and calcite, several aluminosilicate phases can be observed: albite (BT and UND), illite (NA), phengite (RC and UND), cordierite (NA and RA), clinochlore (RC, RA, NA and UND) and muscovite (RA and BT). In addition, iron and magnesium silicate phases were detected as well, including enstatite (RC, RA and NA), lizardite (RC and NA), antigorite (RA and UND) and diopside (RA and NA). Some of the CDW constituents contain minerals from the mica-group, such as phengite and muscovite. The presence of these silicates confirms the potential for alkaline activation of all these powders (Zaharaki et al., 2016). In particular, the mica group minerals exhibit the highest reactivity under alkaline conditions, among the aluminosilicate phases (Choquette et al., 1991).

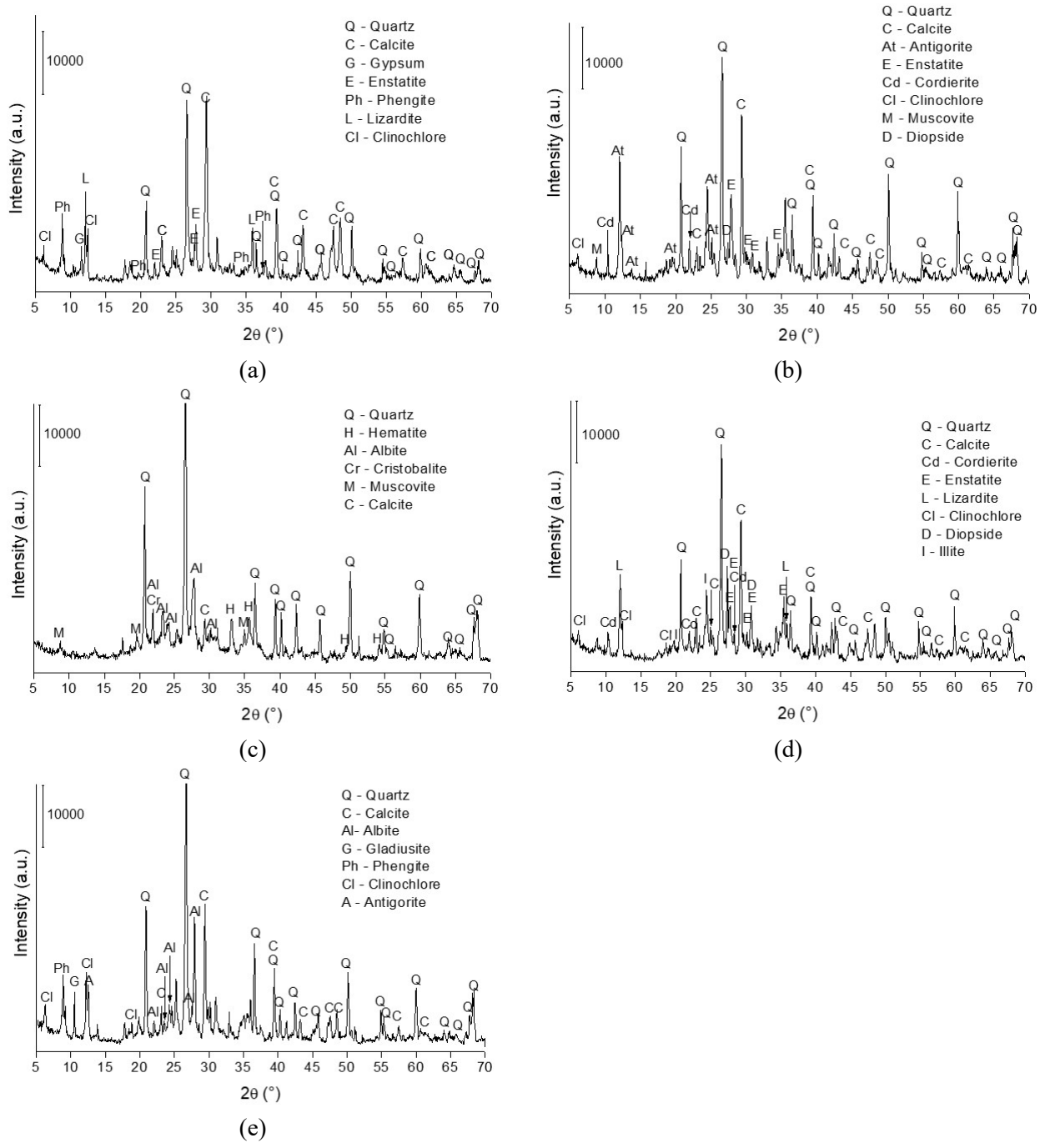

Figure 5. XRD patterns of (a) RC, (b) RA, (c) BT, (d) NA and (e) UND.

Table 2 reports the results of the semi-quantitative phase analysis, expressed as a percentage (of the full mixtures) of aluminosilicate phases, minerals from the mica-group, carbonates and quartz. BT and UND contain a higher amount of either aluminosilicates or mica-group minerals, while RC is richer in carbonate phase. It is worth noting that UND is not characterized by a weighted average composition of the other four constituents. This is plausible since UND may include fine particles of soils and other small material components different from those of the coarser grains used to produce RC, RA, BT and NA fines. Moreover,

since UND was obtained by sieving CDW aggregates at 125 μm, these quantities could not be assessed (Section 2.1).

The XRF results for the five constituent materials are reported in Table 3. First, all the fractions contain a significant amount of silica and alumina, suggesting their possible activation under alkaline conditions. Second, the highest amount of these oxides has been determined in BT, as would be expected from clay-derived construction materials and related waste. The BT sample also contains the highest amount of iron, which accounts for the reddish appearance of the BT fines. Calcium oxide was present in all the constituents too, with the highest amount in RC, a finding which one can reasonably attribute to the presence of calcium-rich aggregates and residual cement.

Table 2. Mineral phases, expressed as a % (of the whole mixtures) of the five constituents

Mineral phases (%)	RC	RA	BT	NA	UND
Aluminosilicates	23	30	64	30	57
Minerals from mica-group	15	12	30	n.a.	23
Carbonates	26	14	6	17	12
Quartz	9	10	22	9	15

Table 3. XRF results for the five constituents (components with a mass smaller than 1% have been omitted)

Component (%)	RC	RA	BT	NA	UND
SiO_2	32.90	36.39	56.40	44.30	42.60
Al_2O_3	6.31	6.34	18.61	8.41	12.80
CaO	24.80	4.12	4.14	11.20	11.50
CO_2	23.44	38.70	1.20	16.87	15.90
Fe_2O_3	4.29	3.69	10.40	5.85	6.84
MgO	4.93	6.92	4.19	10.60	6.00
SO_3	1.42	1.22	0.14	0.20	0.59
K_2O	1.08	1.10	3.05	1.43	2.19
TiO_2	0.43	0.31	1.25	0.46	0.76

3.3 Paste development, viscosity, and pH

Pastes were first prepared at a l/s ratio of 0.6, and their pH values measured. The formulations realized with the more concentrated solution (sol_100%) exhibited a pH value in the range 12.1-12.4, which decreased to values in the range 10.1-11.1 for the pastes with the more diluted AS (sol_50%). Figure 6 exhibits the different viscosities as a function of the rotation speed (on a log scale) measured on the fifteen combinations resulting from the five powders and the AS at the three different concentrations. Results clearly highlight the high viscosity of pastes containing sol_100% and the decrease in viscosity exhibited by those with the more diluted AS. Further differences in rheological behaviour can be ascribed to the single components, taking into consideration that different factors, such as composition, particle size and specific surface area can affect the paste viscosity. UND exhibited the highest viscosity, probably due to its slightly finer particle size. The lowest value, in the entire rotation speed range, was recorded for NA, and imputed to the smooth surface (Figure 4) of the particles, leading to a lower specific surface area of this fraction compared to the other ones. RA, despite

having the largest particle size distribution (Figure 3), shows a moderately high viscosity over the investigated shear range, probably due to the residual bitumen phase which can affect rheological behaviour. In fact, the viscosity of asphalt binders normally ranges from 400 to 2000 CP in the 100-135°C thermal range (Fernandes et al., 2008; Li et al., 2016; Ali et al., 2013), but these values increase exponentially by decreasing the testing temperature (Saboo and Kumar, 2016).

Despite exhibiting high viscosities, all pastes were sufficiently fluid to be poured into the moulds. Furthermore, almost all the samples prepared with l/s = 0.6 exhibited bleeding phenomena, and hardening times longer than 3 days. This behaviour is certainly a consequence of the excessive liquid content. Thus, to avoid bleeding and to shorten the hardening time to 1 day, it was necessary to reduce the l/s ratio to 0.4.

Under such conditions, the fresh materials exhibited the consistency of plastic fine compounds, so a viscosity test could not be carried out (apparent viscosity outside the instrumental measuring range). This consistency was considered appropriate for the preparation of the samples and, therefore, specimens for mechanical characterization were prepared by adopting a l/s ratio of 0.4.

After mechanical tests, the pH values for eluates of alkali-activated powders with sol_100% were measured as per the BS 1377-3 (British Standards Institution, 2018) by means of a pH-meter (Eutech Instruments pH 510). The same pH measurements were carried out on eluates of raw fines (before alkaline activation) for comparison purposes. Higher pH values were observed in eluates of reacted products due to the addition of sol_100% into the material. In the latter case, RC, RA, BT, NA, and UND samples reached pH values of 11.8, 12.2, 11.3, 12.2, and 11.9 respectively, while the pH values for the fines before activation were equal to 10.3, 11.1, 9.5, 10.3, and 10.2.

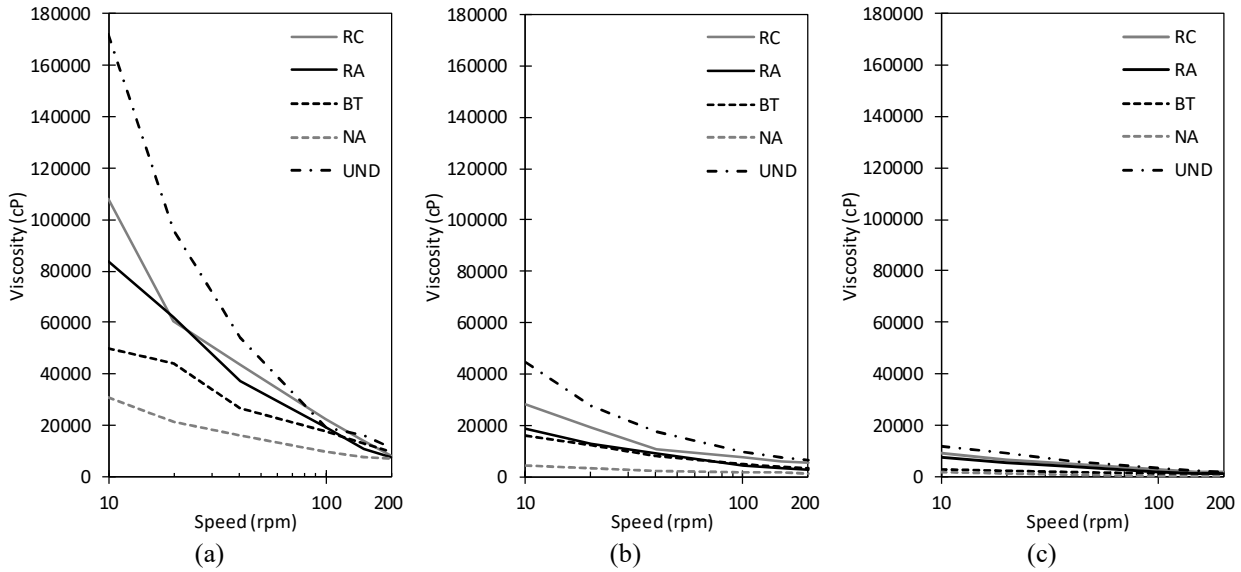

Figure 6. Viscosity of pastes with sol_100% (a), sol_75% (b), and sol_50% (c) and l/s ratio of 0.6.

3.4 Physical and mechanical properties

In Figure 7, the density of the AA pastes is depicted, showing a similar trend to the raw powders bulk density (Table 1). Here, the highest density, independently of the curing time and the AS concentration, was generally achieved by NA (values in the range 1870-2090 kg/m^3), as a result of high aggregate bulk density and good compaction behaviour in the presence of the alkaline solution.

As expected, the lowest values were determined for RC and RA components (values in the range 1730-1880 kg/m^3 for both compositions), due to residual cement paste and organic phase, respectively. Finally, intermediate values were determined for UND and BT, with values in the range 1760-1930 kg/m^3 and 1730-1890 kg/m^3, respectively. The slight decrease in density with curing time was imputed to a progressive water loss, and was more pronounced in the case of materials obtained with the more diluted solution (sol_50%).

Once again, RA showed a good compaction behaviour. In fact, starting from the average bulk density of each raw powder (Table 1) and the density of the AS (precisely, 1.4, 1.3 and 1.2 g/mL for sol_100%, sol_75% and sol_50%, respectively), the theoretical density of each paste was assessed. By considering the samples prepared with sol_100% and cured for 28 days, NA reached 90.2% of its theoretical value, while lower densities (86.1% and 87.4%) were recorded for BT and RC. The highest value, corresponding to 95.0% was achieved by RA, while the intermediate value of 91.0% was determined for UND.

Figure 8 reports the average flexural (Figures 8a, 8b, and 8c) and compressive (Figures 8d, 8e, and 8f) strength values for pastes after 3, 7 and 28 days of curing. An improvement in both flexural and compressive strength values with curing time is evident, consistent with literature referring to AA CDW fines (Komnitsas et al., 2015). Furthermore, the average flexural strength is only 30% of the compressive strength, so the two series of graphs exhibit the same trend but on a different scale.

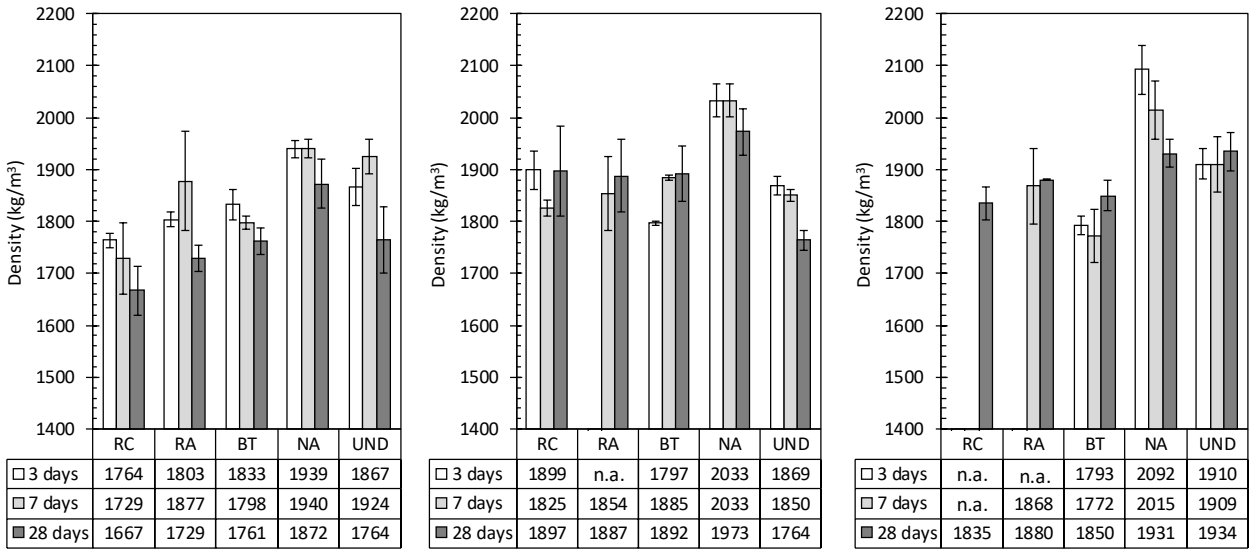

(a) (b) (c)

Figure 7. Density of pastes with (a) sol_0%, (b) sol_75%, and (c) sol_100%. Error bars indicate one standard deviation.

It should be noted that samples of RAsol_100% and RCsol_75% after 3 days of curing, and samples of RCsol_100% after 3 and 7 days proved impossible to test due to their excessive fragility. A visual inspection showed that the hardened samples were weakly bonded and unable to support their own weight (in fact, no results are reported in Figure 8 for these solid-liquid combinations, and no density data are collected in Figure 7).

Samples activated with sol_50% always showed lower flexural and compressive strength values than the corresponding samples containing the two more concentrated solutions (sol_75% and sol_100%). This behaviour cannot be attributed to significant differences in density values, since data collected in Figure 7 showed a moderate density increment for NA and quite similar values for the other components when moving from sol_50% to sol_100%. Thus, it is reasonable to attribute the poor mechanical behaviour of the pastes activated with sol_50% to a not sufficiently basic environment (as reported in Section 3.3), one which does not facilitate a proper aluminosilicate species dissolution and thus geopolymer reactions. In the case of specimens prepared with sol_75% and sol_100%, mechanical data were significantly higher, thus supporting the hypothesis that the AA of CDW fines allows the development of a binding phase which may be exploited for stabilization purposes.

However, clear differences in mechanical properties depending on constituent type and AS concentration were observed. The mechanical behaviour of samples activated with sol_75% may be related to the mineral composition of the constituents. BT and UND, which contain the highest fractions of aluminosilicate phases and, in particular, of highly reactive mica-group phases (Table 2), present the highest flexural and compressive strength values. This evidence is supported by the lower mechanical strengths achieved by NA and RA, which are characterized by an aluminosilicate content which is almost half that of BT and UND.

For RC, a more complex composition properties relationship can be postulated. It presents the highest calcite fraction which can undergo dissolution and corrosion phenomena under alkaline conditions (Choquette et al., 1991). The solubilized calcium, as well as residual unreacted silicates in waste concrete, can give rise to traditional calcium silicate hydrate (CSH), thanks to the presence of water and silicon species in the diluted alkaline activator (Khale and Chaudhary, 2007).

When moving to the mechanical data of RC pastes activated with sol_100%, a significant decrease in mechanical strength was observed, suggesting a lack of free water in this highly concentrated solution, thus impeding the hydration and formation of CSH species. Therefore, RC recorded an optimal performance when activated with sol_75%, reaching flexural and compressive strength values of 1.3 MPa and 3.6 MPa, respectively.

Although RA constituent did not react after 3 days, its samples were found to be significantly active with sol_100% after 28 days of curing, exhibiting relevant flexural strength (4.5 MPa) and compressive strength values (7.9 MPa). This optimal behaviour could be partly attributable to the lower porosity of compacted powders, as evidenced by the Rigden test results in Table 1 and further supported by the high

relative density achieved by the alkali-activated pastes, as previously discussed. However, the high mechanical values of this sample require further experimental investigation to understand if other solid-liquid interaction mechanisms have participated in the alkali reaction.

BT and NA pastes demonstrated a similar evolution in strength with both sol_75% and sol_100%, albeit with sol_75% the two constituents reached even higher strength values. After 28 days of curing, BT achieved a flexural strength of 1.7 MPa and a compressive strength of 4.6 MPa, while NA reached values of 1.0 MPa and 2.5 MPa, respectively.

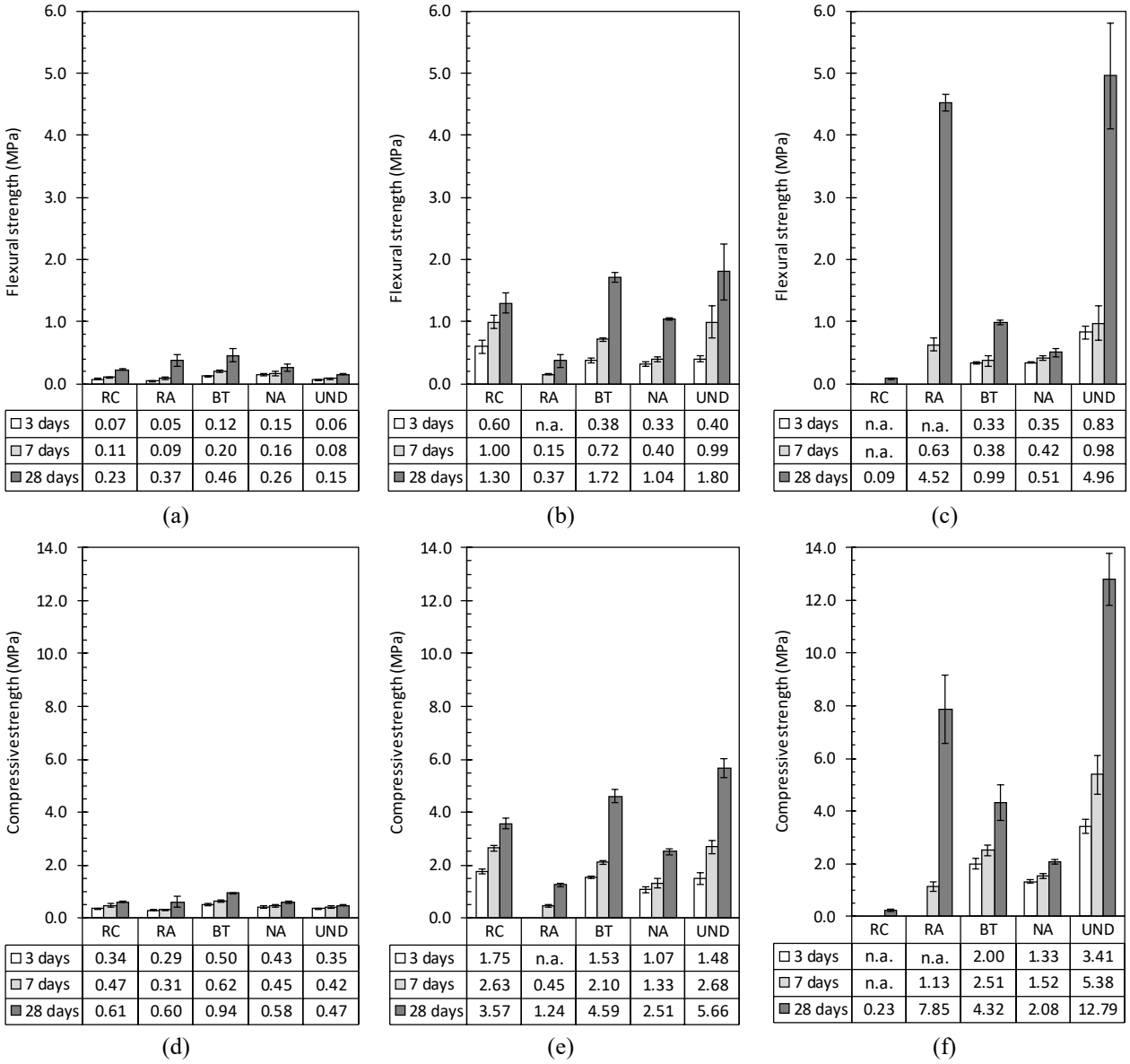

Figure 8. Flexural (from a to c) and compressive (from d to f) strength values of the five CDW constituents mixed with AS at different concentrations: sol_50% (a and d), sol_75% (b and e), and sol_100% (c and f) after 3, 7, and 28 curing days. Error bars indicate one standard deviation.

In contrast, when moving from sol_75% to sol_100%, UND showed a significant mechanical improvement, especially after 28 days of curing. Under these conditions, UND samples exhibited the highest strength in comparison to those recorded for the four main CDW constituents, with a flexural strength of 5.0 MPa and a compressive strength of 12.8 MPa. On the one hand, this remarkable behaviour could be imputed to a good compaction behaviour, as proved by the high relative density of the hardened pastes. On the other hand, it could be postulated that in this fraction an optimal mineral composition was present, with a good balance between calcium and aluminosilicate phases, which led to a strengthening effect due to both aluminosilicate geopolymers and CSH species.

3.5 FESEM analysis

The fracture surfaces of the hardened samples (all of them produced with sol_100% and cured for 28 days) are displayed in Figure 9. In the case of NA and BT, a highly compact and homogeneous microstructure is visible, in which unreacted particles are rarely observed, probably due to an excess of the alkaline solution and related binder phase, which fully cover most of the grains. This hypothesis is supported by the mechanical data, which show comparable results for these two constituents when moving from sol_75% to sol_100%. In the case of RA and UND, we can still observe a well compacted structure, in which some well faceted particles are evident.

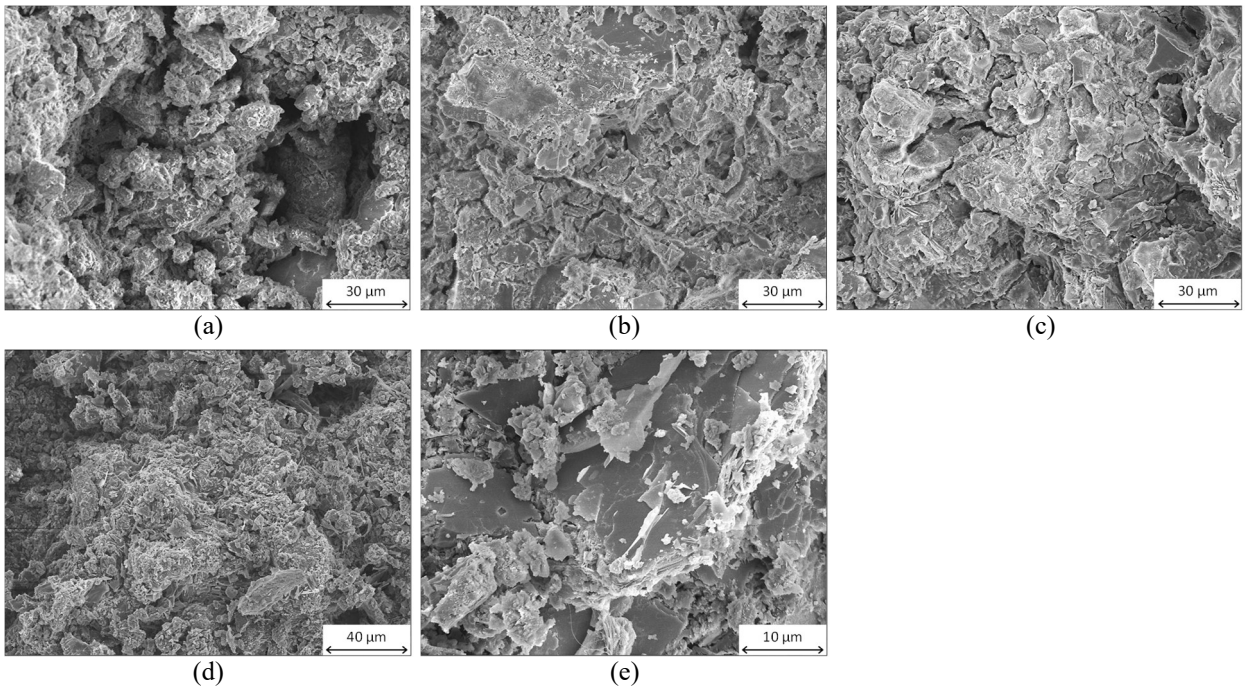

Figure 9. FESEM micrographs of the fracture surface of (a) RC, (b) RA, (c) BT, (d) NA, and (e) UND hardened pastes, obtained by alkaline activation with sol_100% and cured at 28 days.

In particular, the higher magnification image of UND shows the presence of micronic unreacted particles surrounded by a finer matrix, which could be imputed to the geo-polymerization process. A good interface between particles and matrix is observed as well, accounting for the excellent mechanical properties of this material. Finally, a completely different microstructure presented by RC is evident, since loose and unbounded grains are observed, producing a highly porous and inhomogeneous paste, in keeping with the poor mechanical strength demonstrated.

Additional FESEM analyses, together with EDX microanalysis, were carried out on the most representative samples. For instance, in Figure 10 (referred to as UND reacted with sol_100%) a micronic quartz particle (as derived by EDX analysis) embedded in a fine-grained matrix is evidenced. It can be observed that the fine-grained binder phase adheres well to the particle, and no voids or major defects have been detected at their interface. The point analyses performed on different areas around the grain (see for instance point B in Figure 10) systematically showed a Ca-enrichment. In fact, besides the expected high amounts of Si and Na elements, due to the added alkaline solution, Ca, Mg and Al were also detected, suggesting their dissolution in the alkaline medium, thus contributing to the composition of the binding phase. This hypothesis is supported by previous scientific literature related to the alkaline activation of well crystallized Si-Al mineral compounds, as in the present case. Xu and Van Deventer (2000, 2003) investigated the alkaline activation behaviour of 15 natural Al–Si minerals and demonstrated that they are all soluble to some degree in concentrated alkaline solutions, even at room temperature. Choquette et al. (1991) investigated the reactivity of quartz and other crystalline siliceous species under alkaline conditions. These authors reported an increase in the solubility of quartz when they increased the pH (of the alkaline solution) to a value of 12.5. However, the solubility of quartz was designated as light, while other aluminosilicates, like biotite, and other species belonging to the mica group, showed a higher reactivity. The same authors also observed an important reaction of calcite and dolomite phases in the alkaline environment. As speculated in Xu and Van Deventer (2000), alumino-silicate minerals react with the alkaline solution to form a gel-like layer on their surfaces. This gel then diffuses from the particle surface into larger interstitial spaces between the particles, with the precipitation of gel and concurrent dissolution of a new solid. When the gel phase hardens, the non-reacting particles end up bound together, and act as a matrix reinforcement.

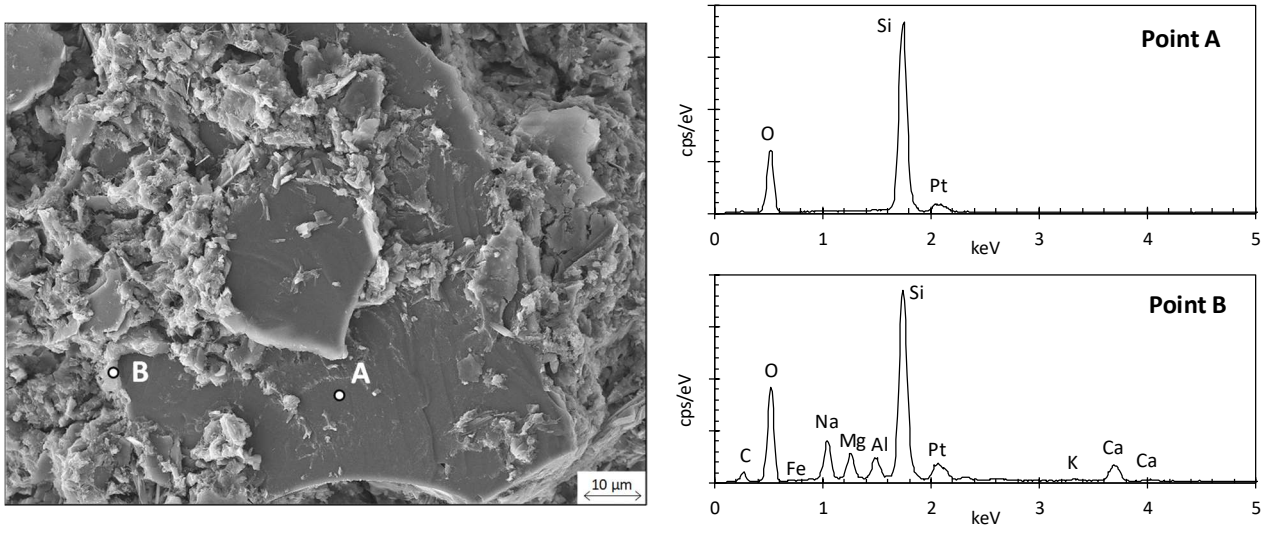

Figure 10. FESEM/EDX analysis of reacted UND material, showing a micronic quartz particle well embedded in a fine-grained binder phase. Results of point analysis in A and B are displayed on the right. The presence of Platinum (Pt) is due to metallization to create a conductive thin film indispensable for FESEM analysis.

A second example, still related to reacted UND fine, is presented in Figure 11. Also in this case, a micronic-sized particle well embedded in a finer matrix can be observed. Following EDX analysis, the $Si_{15.0}Al_{9.3}K_{2.6}Fe_{1.25}Mg_{1.1}O_{70.7}$ elemental composition was determined, suggesting that the particle belongs to the mica group of phengite minerals (Li et al., 2011). Most interesting was the EDX analysis carried out along the lines depicted in Figure 11. Even though the profiles of several elements were acquired, only the ones relating to Si, Al, Na and Ca have been reported here. Si and Al show an almost constant concentration inside the particle, confirming its aluminosilicate composition. Si, in a less regular way, was still detected outside the particle. Na, not detected inside the grain, was clearly present all around the grain, confirming that a Si-Na-based binder phase formed and surrounded the mineral grain. Interestingly, Al and Ca were also detected in the binder, suggesting their dissolution from other species and their diffusion within the matrix and consequent contribution to the composition of the matrix phase.

Some other peculiar microstructural features were observed in the post-reaction samples, and especially in RC and UND. In fact, in both materials, fine grained particles, of a few microns in size, were observed (see for instance Figure 12 for RC reacted sample). Elemental analysis carried out on the single particles showed an enrichment of Ca and Si. This indicated a partial dissolution of calcite under alkaline conditions (Choquette et al. 1991) and a re-precipitation of fine-grained calcite and/or calcium silicate phases in the materials, suggesting a strengthening effect which may be attributable to these fine precipitates. As a final observation, in some RC reacted samples activated with sol_50%, some acicular grains were also observed, as shown in Figure 13. EDX analysis revealed the presence of Si and Na together with a prevalent concentration of Ca, which would suggest the formation of hydrated calcium silicates and/or calcium sodium silicate species, as a result of residual cement hydration and the alkaline reaction of the dissolved calcium species. It should be mentioned, however, that XRD analyses (not shown) carried out on the reacted samples

did not result in the identification of any new Si-Ca species, probably due to the negligible amounts of these species present in the samples or their crystallinity.

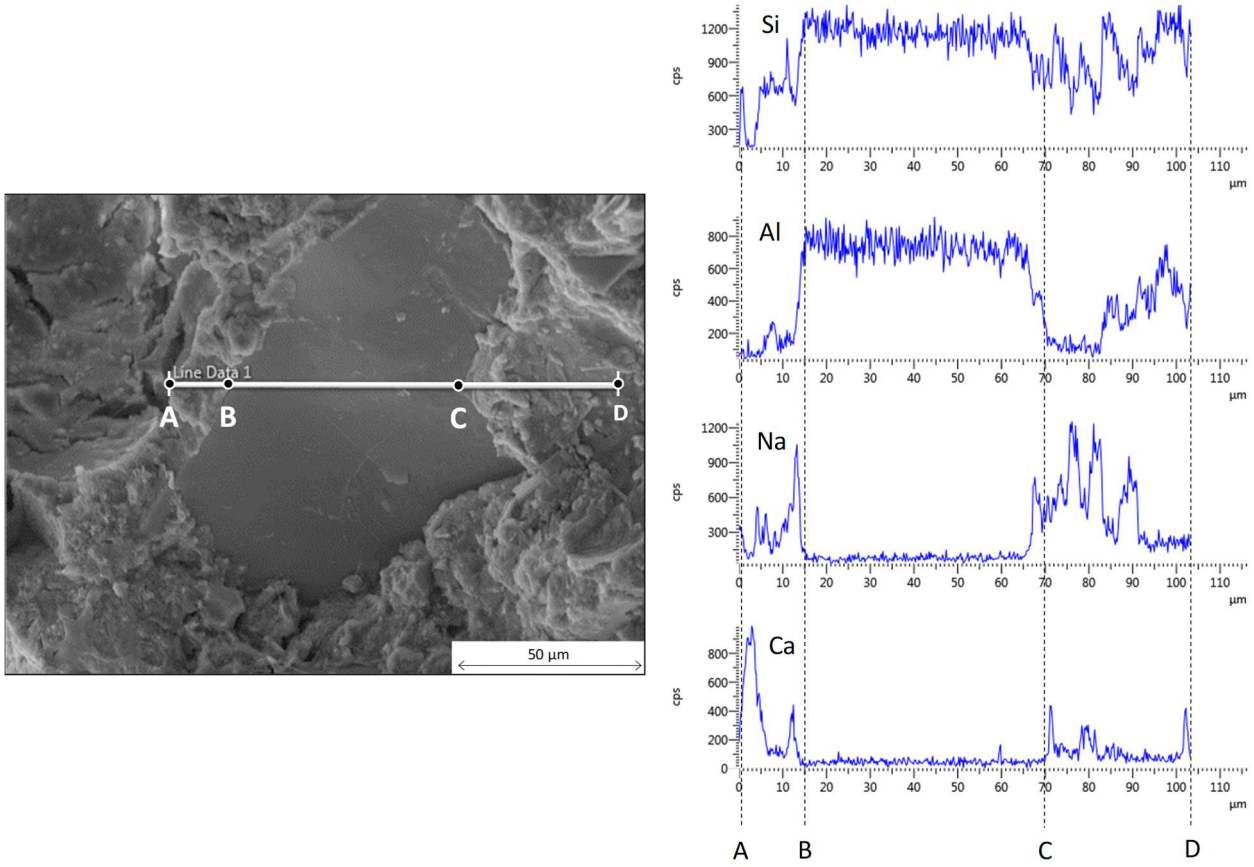

Figure 11. FESEM micrograph of a mineral particle in the activated UND sample and related elemental (Si, Al, Na and Ca) EDX profile inside the particle.

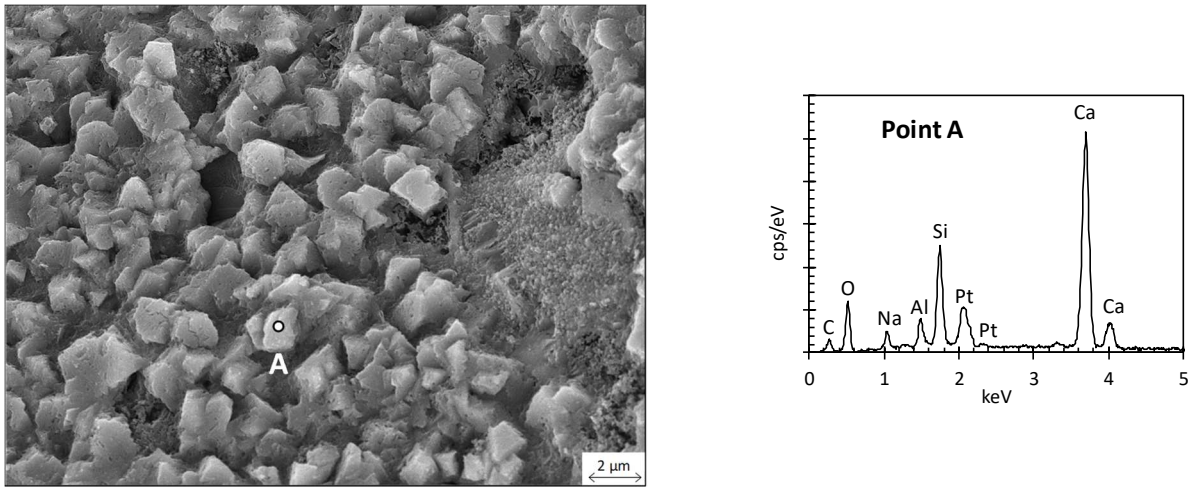

Figure 12. FESEM micrograph of reacted RC sample, and related elemental (Si, Al, Na and Ca) EDX profile inside the particle. The presence of Platinum (Pt) is due to metallization to create a conductive thin film indispensable for FESEM analysis.

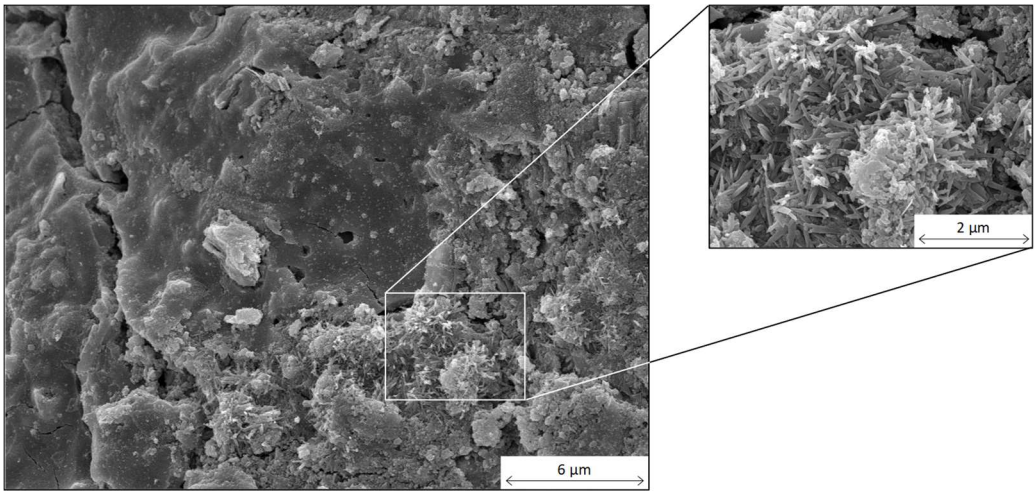

Figure 13. FESEM micrograph of reacted RC sample, showing the presence of acicular grains.

4. CONCLUSIONS AND PERSPECTIVES

This research aimed at investigating the effects of a range of alkali solutions (AS) with different concentrations on fine particles from unselected CDW aggregates. Five powders, one from the fines naturally present in CDW aggregates (named UND), and four from the milling of the four main CDW constituent materials (recycled concrete RC, recycled asphalt RA, crushed bricks and tiles BT, and natural aggregate and excavated soils NA) were investigated. Their preliminary chemical analysis consistently revealed the presence of aluminosilicates, which prove reactive during the alkaline activation process. Results demonstrated that the AS concentration played a key role in the mechanical behaviour of hardened pastes, since 50% concentrated AS (sol_50%) resulted in hardened products with strength values which were significantly lower than those for samples mixed with AS at 75% and 100% concentration levels.

In addition, each constituent displayed a different reactivity behaviour as evidenced by the evolution of compressive and flexural strength values measured on hardened pastes at different curing times. The highest mechanical strength was exhibited by the UND sample (5.0 MPa of flexural strength and 12.8 MPa of compressive strength after 28 days of curing), with encouraging prospects for the use of fines naturally present in CDW granular material as an alternative and more sustainable option for the stabilization of CDW aggregates.

These results demonstrated that CDW fine powders, with particles smaller than 125 µm, tend to react positively in an alkaline environment, increasing in strength without any thermal treatment. They can have a practical application when used for the stabilization of pavement layers made from CDW aggregates without the addition of any ordinary binder (e.g., cement, bitumen). In this case, the fines can be used to stabilize coarser CDW aggregates for the formation of base and subbase layers of road pavements. The technology implies the combination of unselected CDW aggregates with small quantities of AS, which is possible at the construction site as per the use of common soil stabilizers. These machines are used to improve the strength and bearing capacity of any kind of granular material. They can distribute any kind of binding agent (in this

case the alkaline solution) into their mixing chamber, which is then moved along the construction site to lay a course of improved (stabilized) material. After compaction, the added binding agent initiates the hardening process without any specific thermal treatment. Therefore, no thermal treatment was considered in this investigation although it is par for the course (and, indeed, sometimes necessary) for geo-polymerized materials.

As a result, the proposed technology is consistent with the most advanced, sustainable engineering principles since it does not require the use of industrial binders, does not alter the common practice of material treatment and laying operations, and reuses waste materials otherwise destined for landfill sites.

ACKNOWLEDGEMENTS

The authors wish to thank Mr. Cristiano Bertello for his support with part of this research activity. The UCDW aggregates were provided by Cavit S.p.A. operating in the Turin area (North-west of Italy), while the alkaline solution was provided by INGESSIL S.r.l. (Verona), all of which are gratefully acknowledged for their cooperation and continuous support.

REFERENCES

Acosta Alvarez, D., Alonso Aenlle, A., Tenza-Abril, A., 2018. Laboratory Evaluation of Hot Asphalt Concrete Properties with Cuban Recycled Concrete Aggregates. Sustainability 10, 2590. https://doi.org/10.3390/su10082590

Agrela, F., Barbudo, A., Ramírez, A., Ayuso, J., Carvajal, M.D., Jiménez, J.R., 2012. Construction of road sections using mixed recycled aggregates treated with cement in Malaga, Spain. Resour. Conserv. Recycl. 58, 98–106. https://doi.org/10.1016/j.resconrec.2011.11.003

Ali, A.H., Mashaan, N.S., Karim, M.R., 2013. Investigations of Physical and Rheological Properties of Aged Rubberised Bitumen. Adv. Mater. Sci. Eng. 2013, 1–7. https://doi.org/10.1155/2013/239036

Allahverdi, A., Kani, E.N., 2009. Construction wastes as raw materials for geopolymer binders. Int J Civ. Eng 7, 154–160.

Arulrajah, A., Mohammadinia, A., D'Amico, A., Horpibulsuk, S., 2017. Cement kiln dust and fly ash blends as an alternative binder for the stabilization of demolition aggregates. Constr. Build. Mater. 145, 218–225. https://doi.org/10.1016/j.conbuildmat.2017.04.007

Arulrajah, A., Mohammadinia, A., Phummiphan, I., Horpibulsuk, S., Samingthong, W., 2016. Stabilization of Recycled Demolition Aggregates by Geopolymers comprising Calcium Carbide Residue, Fly Ash and Slag precursors. Constr. Build. Mater. 114, 864–873. https://doi.org/10.1016/j.conbuildmat.2016.03.150

Arulrajah, A., Piratheepan, J., Disfani, M.M., Bo, M.W., 2013. Resilient Moduli Response of Recycled Construction and Demolition Materials in Pavement Subbase Applications. J. Mater. Civ. Eng. 25, 1920–1928. https://doi.org/10.1061/(ASCE)MT.1943-5533.0000766

Assi, L.N., Eddie Deaver, E., Ziehl, P., 2018. Effect of source and particle size distribution on the mechanical and microstructural properties of fly Ash-Based geopolymer concrete. Constr. Build. Mater. 167, 372–380. https://doi.org/10.1016/j.conbuildmat.2018.01.193

Bassani, M., Riviera, P.P., Tefa, L., 2016. Short-Term and Long-Term Effects of Cement Kiln Dust Stabilization of Construction and Demolition Waste. J. Mater. Civ. Eng. 29, 04016286. https://doi.org/10.1061/(ASCE)MT.1943-5533.0001797

Bassani, M., Tefa, L., Russo, A., Palmero, P., 2019. Alkali-activation of recycled construction and demolition waste aggregate with no added binder. Constr. Build. Mater. 205, 398–413. https://doi.org/10.1016/j.conbuildmat.2019.02.031

Bennert, T., Papp Jr, W., Maher, A., Gucunski, N., 2000. Utilization of construction and demolition debris under traffic-type loading in base and subbase applications. Transp. Res. Rec. J. Transp. Res. Board 33–39.

Bondar, D., Nanukuttan, S., Provis, J. L., & Soutsos, M., 2019. Efficient mix design of alkali activated slag concretes based on packing fraction of ingredients and paste thickness. J. Clean. Prod. 218, 438-449. https://doi.org/10.1016/j.jclepro.2019.01.332

British Standards Institution, 2018. Methods of test for soils for civil engineering purposes. Part 3: chemical and electro-chemical testing, BS 1377-3:2018.

Cardoso, R., Silva, R.V., Brito, J. de, Dhir, R., 2016. Use of recycled aggregates from construction and demolition waste in geotechnical applications: A literature review. Waste Manag. 49, 131–145. https://doi.org/10.1016/j.wasman.2015.12.021

CIRS (Centro Interuniversitario Sperimentale di Ricerca Stradale), 2001. Norme Tecniche Prestazionali per Capitolati Speciali d'Appalto (*in Italian*).

Chen, Q., Zhang, Q., Xiao, C., Chen, X., 2017. Backfilling behavior of a mixed aggregate based on construction waste and ultrafine tailings. PLOS ONE 12, e0179872. https://doi.org/10.1371/journal.pone.0179872

Choquette, M., Berube, M.-A., Locat, J., 1991. Behavior of common rock-forming minerals in a strongly basic NaOH solution. Can. Mineral. 29, 163–173.

Contreras, M., Teixeira, S.R., Lucas, M.C., Lima, L.C.N., Cardoso, D.S.L., da Silva, G.A.C., Gregório, G.C., de Souza, A.E., dos Santos, A., 2016. Recycling of construction and demolition waste for producing new construction material (Brazil case-study). Constr. Build. Mater. 123, 594–600. https://doi.org/10.1016/j.conbuildmat.2016.07.044

Del Rey, I., Ayuso, J., Galvín, A., Jiménez, J., Barbudo, A., 2016a. Feasibility of Using Unbound Mixed Recycled Aggregates from CDW over Expansive Clay Subgrade in Unpaved Rural Roads. Materials 9, 931. https://doi.org/10.3390/ma9110931

Del Rey, I., Ayuso, J., Barbudo, A., Galvín, A.P., Agrela, F., de Brito, J., 2016b. Feasibility study of cement-treated 0–8 mm recycled aggregates from construction and demolition waste as road base layer. Road Mater. Pavement Des. 17, 678–692. https://doi.org/10.1080/14680629.2015.1108221

Duxson, P., Fernández-Jiménez, A., Provis, J.L., Lukey, G.C., Palomo, A., van Deventer, J.S.J., 2007a. Geopolymer technology: the current state of the art. J. Mater. Sci. 42, 2917–2933. https://doi.org/10.1007/s10853-006-0637-z

Duxson, P., Provis, J.L., Lukey, G.C., van Deventer, J.S.J., 2007b. The role of inorganic polymer technology in the development of 'green concrete.' Cem. Concr. Res. 37, 1590–1597. https://doi.org/10.1016/j.cemconres.2007.08.018

European Commission, 2011. Construction and demolition waste - Environment - European Commission.

European Committee for Standardization, 2008a. Tests for mechanical and physical properties of aggregates - Part 7: Determination of the particle density of filler - Pyknometer method, EN 1097-7:2008.

European Committee for Standardization, 2008b. Tests for mechanical and physical properties of aggregates - Part 4: Determination of the voids of dry compacted filler, EN 1097-4:2008.

European Parliament, 2008. Directive 2008/98/EC of the European Parliament and of the Council of 19 November 2008 on waste and repealing certain directives (waste framework directive). 312(11-2b), 2008/98/EC.

Fernandes, M.R.S., Forte, M.M.C., Leite, L.F.M., 2008. Rheological Evaluation of Polymer-Modified Asphalt Binders. Mater. Res. 11, 6.

Formela, K., Klein, M., Colom, X., Saeb, M.R., 2016. Investigating the combined impact of plasticizer and shear force on the efficiency of low temperature reclaiming of ground tire rubber (GTR). Polym. Degrad. Stab. 125, 1–11. https://doi.org/10.1016/j.polymdegradstab.2015.12.022

Gómez-Meijide, B., Pérez, I., Pasandín, A.R., 2016. Recycled construction and demolition waste in Cold Asphalt Mixtures: evolutionary properties. J. Clean. Prod. 112, 588–598. https://doi.org/10.1016/j.jclepro.2015.08.038

Gonzalez-Corominas, A., Etxeberria, M., Poon, C., 2017. Influence of the Quality of Recycled Aggregates on the Mechanical and Durability Properties of High Performance Concrete. Waste Biomass Valorization 8, 1421–1432. https://doi.org/10.1007/s12649-016-9637-7

Hoy, M., Horpibulsuk, S., Arulrajah, A., 2016. Strength development of Recycled Asphalt Pavement – Fly ash geopolymer as a road construction material. Constr. Build. Mater. 117, 209–219. https://doi.org/10.1016/j.conbuildmat.2016.04.136

Humad, A. M., Kothari, A., Provis, J. L., & Cwirzen, A. 2019. The effect of blast furnace slag/fly ash ratio on setting, strength, and shrinkage of alkali-activated pastes and concretes. Frontiers in Materials, 6. 9. https://doi.org/10.3389/fmats.2019.00009

Jamieson, E., McLellan, B., van Riessen, A., Nikraz, H., 2015. Comparison of embodied energies of Ordinary Portland Cement with Bayer-derived geopolymer products. J. Clean. Prod. 99, 112–118. https://doi.org/10.1016/j.jclepro.2015.03.008

Jiménez, J.R., Ayuso, J., Agrela, F., López, M., Galvín, A.P., 2012. Utilisation of unbound recycled aggregates from selected CDW in unpaved rural roads. Resour. Conserv. Recycl. 58, 88–97. https://doi.org/10.1016/j.resconrec.2011.10.012

Jiménez, J.R., 2013. Recycled aggregates (RAs) for roads, in: Handbook of Recycled Concrete and Demolition Waste. Elsevier, pp. 351–377. https://doi.org/10.1533/9780857096906.3.351

Juan-Valdés, A., Rodríguez-Robles, D., García-González, J., Guerra-Romero, M.I., Morán-del Pozo, J.M., 2018. Mechanical and microstructural characterization of non-structural precast concrete made with recycled mixed ceramic aggregates from construction and demolition wastes. J. Clean. Prod. 180, 482–493. https://doi.org/10.1016/j.jclepro.2018.01.191

Katz, A., 2003. Properties of concrete made with recycled aggregate from partially hydrated old concrete. Cem. Concr. Res. 33, 703–711. https://doi.org/10.1016/S0008-8846(02)01033-5

Khale, D., Chaudhary, R., 2007. Mechanism of geopolymerization and factors influencing its development: a review. J. Mater. Sci. 42, 729–746. https://doi.org/10.1007/s10853-006-0401-4

Kishchynskyi, S., Nagaychuk, V., Bezuglyi, A., 2016. Improving Quality and Durability of Bitumen and Asphalt Concrete by Modification Using Recycled Polyethylene Based Polymer Composition. Procedia Eng. 143, 119–127. https://doi.org/10.1016/j.proeng.2016.06.016

Komnitsas, K., Zaharaki, D., 2007. Geopolymerisation: A review and prospects for the minerals industry. Miner. Eng. 20, 1261–1277. https://doi.org/10.1016/j.mineng.2007.07.011

Komnitsas, K., Zaharaki, D., Vlachou, A., Bartzas, G., Galetakis, M., 2015. Effect of synthesis parameters on the quality of construction and demolition wastes (CDW) geopolymers. Adv. Powder Technol. 26, 368–376. https://doi.org/10.1016/j.apt.2014.11.012

Leite, F. da C., Motta, R. dos S., Vasconcelos, K.L., Bernucci, L., 2011. Laboratory evaluation of recycled construction and demolition waste for pavements. Constr. Build. Mater. 25, 2972–2979. https://doi.org/10.1016/j.conbuildmat.2010.11.105

Li, H., Zhang, L., Christy, A. G. 2011. The correlation between Raman spectra and the mineral composition of muscovite and phengite. In Ultrahigh-Pressure Metamorphism, 187-212, Elsevier. https://doi.org/10.1016/B978-0-12-385144-4.00006-0

Li, R., Wang, C., Wang, P., Pei, J., 2016. Preparation of a novel flow improver and its viscosity-reducing effect on bitumen. Fuel 181, 935–941. https://doi.org/10.1016/j.fuel.2016.05.028

Limbachiya, M.C., Leelawat, T., Dhir, R.K., 2000. Use of recycled concrete aggregate in high-strength concrete. Mater. Struct. 33, 574–580.

Loria, H., Pereira-Almao, P., Satyro, M., 2009. Prediction of Density and Viscosity of Bitumen Using the Peng−Robinson Equation of State. Ind. Eng. Chem. Res. 48, 10129–10135. https://doi.org/10.1021/ie901031n

McLellan, B.C., Williams, R.P., Lay, J., van Riessen, A., Corder, G.D., 2011. Costs and carbon emissions for geopolymer pastes in comparison to ordinary portland cement. J. Clean. Prod. 19, 1080–1090. https://doi.org/10.1016/j.jclepro.2011.02.010

Mhlongo, S.M., Abiola, O.S., Ndambuki, J.M., Kupolati, W.K., 2014. Use of recycled asphalt materials for Sustainable construction and rehabilitation of roads, in: International Conference on Biological, Civil and Environmental Engineering (BCEE-2014) March. Presented at the International Conference on Biological, Civil and Environmental Engineering (BCEE-2014) March, pp. 91–94. https://doi.org/10.15242/IICBE.C0314157

Mohammadinia, A., Arulrajah, A., Sanjayan, J., Disfani, M.M., Bo, M.W., Darmawan, S., 2014. Laboratory Evaluation of the Use of Cement-Treated Construction and Demolition Materials in Pavement Base and Subbase Applications. J. Mater. Civ. Eng. 27, 04014186. https://doi.org/10.1061/(ASCE)MT.1943-5533.0001148

Mohammadinia, A., Arulrajah, A., Sanjayan, J., Disfani, M.M., Win Bo, M., Darmawan, S., 2016. Stabilization of Demolition Materials for Pavement Base/Subbase Applications Using Fly Ash and Slag Geopolymers: Laboratory Investigation. J. Mater. Civ. Eng. 28, 04016033. https://doi.org/10.1061/(ASCE)MT.1943-5533.0001526

Nguyen, L., Moseson, A.J., Farnam, Y., Spatari, S., 2018. Effects of composition and transportation logistics on environmental, energy and cost metrics for the production of alternative cementitious binders. J. Clean. Prod. 185, 628–645. https://doi.org/10.1016/j.jclepro.2018.02.247

Ossa, A., García, J.L., Botero, E., 2016. Use of recycled construction and demolition waste (CDW) aggregates: A sustainable alternative for the pavement construction industry. J. Clean. Prod. 135, 379–386. https://doi.org/10.1016/j.jclepro.2016.06.088

Paranavithana, S., Mohajerani, A., 2006. Effects of recycled concrete aggregates on properties of asphalt concrete. Resour. Conserv. Recycl. 48, 1–12. https://doi.org/10.1016/j.resconrec.2005.12.009

Pasandín, A.R., Pérez, I., 2013. Laboratory evaluation of hot-mix asphalt containing construction and demolition waste. Constr. Build. Mater. 43, 497–505. https://doi.org/10.1016/j.conbuildmat.2013.02.052

Pathak, A., Jha, V.K., 2013. Synthesis of Geopolymer from Inorganic Construction Waste. J. Nepal Chem. Soc. 30, 45–51.

Pitarch, A.M., Reig, L., Tomás, A.E., López, F.J., 2017. Effect of Tiles, Bricks and Ceramic Sanitary-Ware Recycled Aggregates on Structural Concrete Properties. Waste Biomass Valorization. https://doi.org/10.1007/s12649-017-0154-0

Poon, C.S., Chan, D., 2006. Feasible use of recycled concrete aggregates and crushed clay brick as unbound road sub-base. Constr. Build. Mater. 20, 578–585. https://doi.org/10.1016/j.conbuildmat.2005.01.045

Rahman, M.A., Imteaz, M., Arulrajah, A., Disfani, M.M., 2014. Suitability of recycled construction and demolition aggregates as alternative pipe backfilling materials. J. Clean. Prod. 66, 75–84. https://doi.org/10.1016/j.jclepro.2013.11.005

Reig, L., Tashima, M.M., Soriano, L., Borrachero, M.V., Monzó, J., Payá, J., 2013. Alkaline Activation of Ceramic Waste Materials. Waste Biomass Valorization 4, 729–736. https://doi.org/10.1007/s12649-013-9197-z

Robayo-Salazar, R.A., Mejía-Arcila, J.M., Mejía de Gutiérrez, R., 2017. Eco-efficient alkali-activated cement based on red clay brick wastes suitable for the manufacturing of building materials. J. Clean. Prod. 166, 242–252. https://doi.org/10.1016/j.jclepro.2017.07.243

Rodríguez, C., Parra, C., Casado, G., Miñano, I., Albaladejo, F., Benito, F., Sánchez, I., 2016. The incorporation of construction and demolition wastes as recycled mixed aggregates in non-structural concrete precast pieces. J. Clean. Prod. 127, 152–161. https://doi.org/10.1016/j.jclepro.2016.03.137

Roy, D.M., 1999. Alkali-activated cements Opportunities and challenges. Cem. Concr. Res. 6.

Saboo, N., Kumar, P., 2016. Use of flow properties for rheological modeling of bitumen. Int. J. Pavement Res. Technol. 9, 63–72. https://doi.org/10.1016/j.ijprt.2016.01.005

Sangiorgi, C., Lantieri, C., Dondi, G., 2015. Construction and demolition waste recycling: an application for road construction. Int. J. Pavement Eng. 16, 530–537. https://doi.org/10.1080/10298436.2014.943134

Silva, R.V., de Brito, J., Dhir, R.K., 2014. Properties and composition of recycled aggregates from construction and demolition waste suitable for concrete production. Constr. Build. Mater. 65, 201–217. https://doi.org/10.1016/j.conbuildmat.2014.04.117

Temuujin, J., Williams, R.P., van Riessen, A., 2009. Effect of mechanical activation of fly ash on the properties of geopolymer cured at ambient temperature. J. Mater. Process. Technol. 209, 5276–5280. https://doi.org/10.1016/j.jmatprotec.2009.03.016

Tsoumani, A.A., Barkoula, N.-M., Matikas, T.E., 2015. Recycled aggregate as structural material. Waste Biomass Valorization 6, 883–890. https://doi.org/10.1007/s12649-015-9385-0

Vandecasteele, C., Heynen, J., Goumans, H., 2013. Materials Recycling in Construction: A Review of the Last 2 Decades Illustrated by the WASCON Conferences. Waste Biomass Valorization 4, 695–701. https://doi.org/10.1007/s12649-013-9239-6

Vieira, C.S., Pereira, P.M., 2015. Use of recycled construction and demolition materials in geotechnical applications: A review. Resour. Conserv. Recycl. 103, 192–204. https://doi.org/10.1016/j.resconrec.2015.07.023

Wang, L., Cho, D.W., Tsang, D.C., Cao, X., Hou, D., Shen, Z., Alessi, D.S., Ok, Y.S., Poon, C.S. 2019a. Green remediation of As and Pb contaminated soil using cement-free clay-based stabilization/solidification. Environ. Int., 126, 336-345. https://doi.org/10.1016/j.envint.2019.02.057

Wang, L., Chen, L., Cho, D. W., Tsang, D. C., Yang, J., Hou, D., Kitae, B., Harn, W.K., Poon, C. S. 2019b. Novel synergy of Si-rich minerals and reactive MgO for stabilisation/solidification of contaminated sediment. J. Hazard. Mater., 365, 695-706. https://doi.org/10.1016/j.jhazmat.2018.11.067

Xu, H., & Van Deventer, J. S. J. 2000. The geopolymerisation of alumino-silicate minerals. Int. J. Miner. Process., 59(3), 247-266. https://doi.org/10.1016/S0301-7516(99)00074-5

Xu, H., & van Deventer, J. S. 2003. The effect of alkali metals on the formation of geopolymeric gels from alkali-feldspars. Colloid Surface A, 216(1-3), 27-44. https://doi.org/10.1016/S0927-7757(02)00499-5

Zaharaki, D., Galetakis, M., Komnitsas, K., 2016. Valorization of construction and demolition (C&D) and industrial wastes through alkali activation. Constr. Build. Mater. 121, 686–693. https://doi.org/10.1016/j.conbuildmat.2016.06.051

Zedan, S.R., Mohamed, M.R., Ahmed, D.A., Mohammed, A.H., 2015. Effect of demolition/construction wastes on the properties of alkali activated slag cement. HBRC J. https://doi.org/10.1016/j.hbrcj.2015.12.001

Zhou, X., Liu, D., Bu, H., Deng, L., Liu, H., Yuan, P., Du, P., Song, H., 2018. XRD-based quantitative analysis of clay minerals using reference intensity ratios, mineral intensity factors, Rietveld, and full pattern summation methods: A critical review. Solid Earth Sci. 3, 16–29. https://doi.org/10.1016/j.sesci.2017.12.002